

# Substrate-Induced Stabilization and Reconstruction of Zigzag Edges in Graphene Nanoislands on Ni(111)

A. Garcia-Lekue,<sup>\*,†,‡</sup> M. Ollé,<sup>\*,§,||</sup> D. Sanchez-Portal,<sup>†,⊥</sup> J. J. Palacios,<sup>#,○</sup> A. Mugarza,<sup>§</sup> G. Ceballos,<sup>§</sup> and P. Gambardella<sup>§,||,□</sup>

<sup>†</sup>Donostia International Physics Center (DIPC), Paseo Manuel de Lardizabal 4, E-20018 San Sebastián, Spain

<sup>‡</sup>IKERBASQUE, Basque Foundation for Science, E- 48011 Bilbao, Spain

<sup>§</sup>Catalan Institute of Nanoscience and Nanotechnology (ICN2), UAB Campus, E-08193 Bellaterra (Barcelona), Spain

<sup>||</sup>Department of Materials, Eidgenössische Technische Hochschule (ETH) Zurich, Hönggerbergstrasse 64, CH-8093 Zurich, Switzerland

<sup>⊥</sup>Centro de Física de Materiales CSIC-UPV/EHU, Paseo Manuel de Lardizabal 5, San Sebastián, Spain

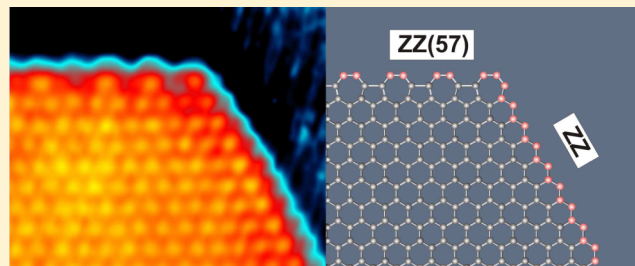
<sup>#</sup>Departamento de Física de la Materia Condensada, Universidad Autónoma de Madrid, Cantoblanco, Madrid 28049, Spain

<sup>○</sup>Instituto de Física de la Materia Condensada (IFIMAC), Universidad Autónoma de Madrid, Cantoblanco, Madrid 28049, Spain

<sup>□</sup>Institució Catalana de Recerca i Estudis Avancats (ICREA), E-08193 Barcelona, Spain

## S Supporting Information

**ABSTRACT:** We combine experimental observations by scanning tunneling microscopy (STM) and density functional theory (DFT) to reveal the most stable edge structures of graphene on Ni(111) as well as the role of stacking-driven activation and suppression of edge reconstruction. Depending on the position of the outermost carbon atoms relative to hollow and on-top Ni sites, zigzag edges have very different energies. Triangular graphene nanoislands are exclusively bound by the more stable zigzag hollow edges. In hexagonal nanoislands, which are constrained by geometry to alternate zigzag hollow and zigzag top edges along their perimeter, only the hollow edge is stable, whereas the top edges spontaneously reconstruct into the (57) pentagon–heptagon structure. Atomically resolved STM images are consistent with either top-fcc or top-hcp epitaxial stacking of graphene and Ni sites, with the former being favored by DFT. Finally, we find that there is a one-to-one relationship between the edge type, graphene stacking, and orientation of the graphene islands.



## INTRODUCTION

Edges play a fundamental role in shaping the morphology<sup>1–5</sup> and electronic<sup>6–9</sup> properties of graphene nanostructures. Electron confinement due to edge boundaries gives rise to energy band gaps,<sup>10,11</sup> localized states,<sup>6,7</sup> spin-polarization,<sup>10,12</sup> and spin-dependent electron scattering.<sup>13</sup> Furthermore, graphene edges determine the preferred sites for the attachment of metal atoms<sup>14</sup> and chemical functionalization,<sup>15</sup> as well as oxygen etching and intercalation.<sup>16,17</sup> Understanding and defining the edge morphology is therefore important to tune the growth of graphene nanostructures as well as to modulate the electronic properties of graphene in confined geometries.

In free-standing graphene, crystallographically oriented edges are of either zigzag (zz) or armchair (ac) type.<sup>6</sup> Graphene with ac and zz edges can be obtained by mechanical exfoliation<sup>18</sup> and etching techniques.<sup>19</sup> However, free-standing unpassivated edges are unstable due to the high density of dangling bonds,<sup>20–22</sup> which induce the zz edges to spontaneously reconstruct into a line of pentagon and heptagon pairs, the so-called zz(57) or Stone–Wales reconstruction.<sup>23,24</sup> A very different scenario arises in epitaxially grown graphene, where

the interaction with the substrate can stabilize ac,<sup>25,26</sup> zz,<sup>27–29</sup> and reconstructed edges<sup>4,30–32</sup> and induce complex graphenemetal boundaries.<sup>28,29,33</sup>

Despite the potential of epitaxy for tailoring graphene edges evidenced by these studies, predicting the edge structure is still a challenging task, which requires detailed insight into the interplay of substrate interaction and edge morphology. For example, minimal variations in the lattice constant and electronic structure of the substrate can lead to very different edge energetics, resulting in hexagonal islands with zz and Klein-type edges in Co(1000),<sup>30</sup> and either hexagonal or triangular islands in Ni(111), depending on growth parameters.<sup>34,35</sup> The latter strongly differ from the quasi-isotropic shape predicted by theory.<sup>4,31</sup>

In this work, we show that the experimentally observed morphological transition of graphene islands on Ni(111) is driven by a substrate-induced reconstruction of zz edges into

Received: November 5, 2014

Revised: February 2, 2015

Published: February 2, 2015



the  $zz(57)$  structure. This reconstruction, which was found to be unstable on most close-packed metals including Ni(111)<sup>4,31</sup> according to previous first-principles calculations,<sup>4,31</sup> occurs along a particular direction with respect to the substrate, and can only be properly reproduced by theory by taking into account the stacking of differently oriented edges.

## METHODS

**Experiments.** Graphene nanoislands were grown on a Ni(111) single-crystal surface kept in a ultrahigh vacuum (UHV) chamber with a base pressure of  $3 \times 10^{-10}$  mbar. The crystal surface was cleaned by repeated cycles of  $\text{Ar}^+$  sputtering followed by annealing at  $800^\circ\text{C}$  during 1 min. The surface temperature was measured throughout the experiment using a pyrometer (IMPAC IGA 140). Propene was dosed on a freshly prepared Ni(111) crystal at room temperature. Once the dosing process is complete, the sample is heated at  $500^\circ\text{C}$  for 5 min to nucleate the graphene nanoislands and subsequently cooled to room temperature. The islands so obtained have an irregular shape. In order to prepare triangular and hexagonal graphene islands (TGIs and HGIs, respectively), we postanneal the sample to a temperature  $T_A = 500^\circ\text{C}$  ( $650^\circ\text{C}$ ) during a time  $t_A = 20$  min (10 min). We use a propene dose  $D = 1$  L for the TGIs and  $D = 2$  L for the HGIs to compensate for C loss at high temperature. The heating rate was  $12^\circ\text{C}/\text{s}$  and the cooling rate was  $1.7^\circ\text{C}/\text{s}$ . It should be emphasized that the presence of contaminants, such as H or CO, is minimized by annealing the samples in UHV. Atomic H, as well as molecular species such as CO, desorbs from Ni(111) at temperatures lower than  $300^\circ\text{C}$ .<sup>36,37</sup> Moreover, we observe that the island shape does not change at  $500^\circ\text{C}$ , which is another indication that the edge structures are not driven by hydrogenation. Although it is notoriously difficult to completely rule out the presence of contaminants, the fact that DFT calculations provide a very satisfactory explanation for the STM observations can be considered as further evidence for the absence of contaminants at the edges. More details on the preparation of TGIs and HGIs can be found in ref 35. Topographic images of the surface were obtained at room temperature using a variable-temperature scanning tunneling microscope (SPECs, STM Aarhus 150) and processed using a freeware software (WSxM 5.0 develop 4.1).<sup>38</sup>

**Theory.** Ab initio spin-polarized calculations were performed using DFT, as implemented in the SIESTA<sup>39</sup> and ANT.G codes.<sup>40</sup> For the description of TGIs using SIESTA, we considered a supercell made of three Ni(111) layers (up to four layers in convergence test, see the Supporting Information) and one graphene island containing 22 C atoms, whereas the results using ANT.G were obtained employing a graphene island of 33 C atoms placed on a Ni(111) surface described by a cluster with 2 Ni layers. The simulation of HGIs with alternate edge types would require the use of extremely large supercells; we have therefore used the nanoribbon geometry to compare the properties of different graphene edges on Ni(111) using SIESTA. The results obtained for the nanoribbon calculations yield information on the edge stability and energetics, which can be extended to the case of large hexagonal nanoislands. For such calculations, we employed a  $4 \times 8$  supercell made of three Ni(111) layers and a graphene ribbon containing 40 C atoms placed on one of the surfaces. In this case, only graphene nanoribbons with top-fcc stacking with respect to the underlying Ni(111) were considered. Further details on the calculations are given in the Supporting Information.

## RESULTS AND DISCUSSION

The small lattice mismatch between graphene and Ni(111),  $1 \times 1$  stacking, and the corresponding absence of a Moiré pattern make this system an optimal candidate to investigate the structure, stability, and epitaxial relationship between the graphene edges and a metallic substrate. Several  $1 \times 1$  stacking structures have been proposed for graphene monolayers on Ni(111).<sup>41–45</sup> According to these previous studies, the top-fcc, top-hcp, and bridge-top configurations are considered to be the most stable, with a small energetic preference for the top-fcc stacking. Indeed, a recent report has confirmed the coexistence of these three graphene configurations on Ni(111), with a general predominance of top-fcc.<sup>46</sup> In the case of graphene nanoislands on Ni(111) reported here, the possible stacking configurations are expected to be the same as for the graphene monolayer. Symmetry arguments, however, allow us to exclude bridge-top stacking (see Supporting Information) and consider only top-fcc and top-hcp stacking shown in Figure 1.

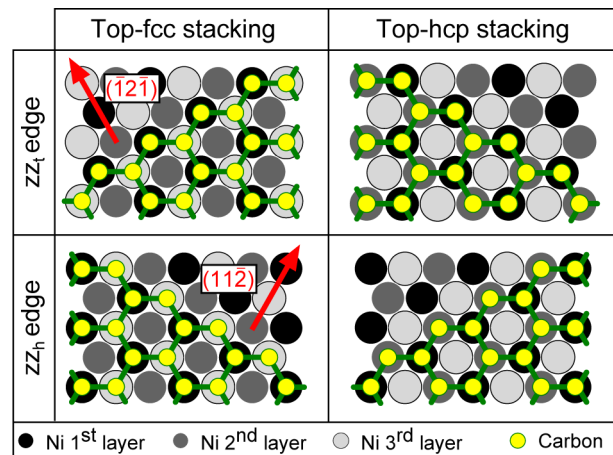


Figure 1. Hard sphere models of different zigzag graphene edges on Ni(111) for fcc (left) and hcp (right) graphene-Ni stacking.

Regarding  $zz$  edges, we distinguish two different types according to the position of the outermost C atoms with respect to the substrate. We thus define edges having the outer C atoms located on top of Ni atoms as  $zz_t$  and edges having the outer C atoms on hollow sites as  $zz_h$ , as shown in Figure 1. The outer C atoms of a  $zz_h$  edge can occupy hollow fcc or hcp sites, depending on the stacking configuration and edge orientation. As seen in Figure 1, the crystallographic directions of  $zz_t$  and  $zz_h$  edges with the same stacking differ by  $60^\circ$  and the crystallographic directions of edges of the same type but different stacking also differ by  $60^\circ$ . Note also that an edge perpendicular to the  $(\overline{1}\overline{2}\overline{1})$  direction can be either a top-fcc/ $zz_t$  or a top-hcp/ $zz_h$  edge, while an edge perpendicular to the  $(1\overline{1}\overline{2})$  direction can be either a top-fcc/ $zz_h$  or a top-hcp/ $zz_t$  edge.

In previous work, we have shown that graphene islands that nucleate with random shape upon dosing propene on a clean Ni(111) surface and annealing the substrate above  $450^\circ\text{C}$  evolve to either triangular or hexagonal shapes depending on the initial hydrocarbon dose, annealing time, and temperature.<sup>35</sup> Such TGIs and HGIs provide an ideal system to study the structure and stacking of the edge C atoms on close-packed metal surfaces. Due to the 3-fold symmetry of the  $zz_t$  and  $zz_h$  edges introduced above, TGIs present only a single-edge type, whereas HGIs must alternate different edges. By varying the

island size and shape, it is thus possible not only to characterize the different edges, but also to study the influence of the edge morphology and graphene stacking on the stability of the islands.

Figure 2a shows a representative STM image of TGIs obtained by annealing the substrate to 500 °C and subsequent

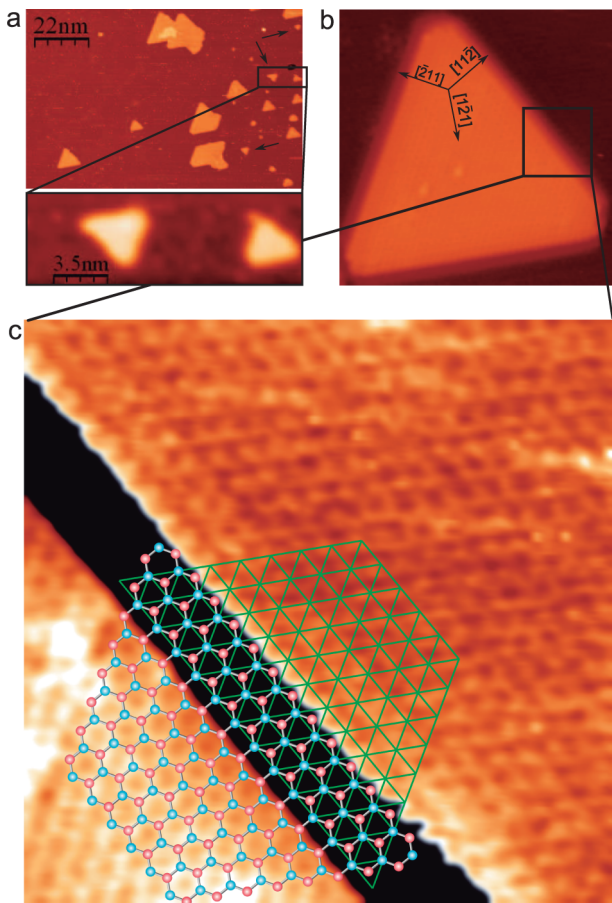


**Figure 2.** (a) STM image of a large sample area with TGIs of different sizes. The enlarged image shows two small TGIs oriented in opposite directions. Set point current and bias voltage:  $I = 1.9 \text{ nA}$ ,  $V_b = 3.7 \text{ mV}$ . (b) STM image of a single TGI. Set point:  $I = 1.0 \text{ nA}$ ,  $V_b = 0.9 \text{ mV}$ . (c) Zoom-in of an edge region with the image contrast set to show the atomic resolution on both graphene and Ni layers. The left part of the image corresponds to the graphene edge with a superposed honeycomb lattice (red and blue circles), the right part to the Ni(111) surface with a superposed hexagonal lattice (green mesh). The black stripe is a transition region related to the finite size of the tip where atomic resolution is missing.

cooling to room temperature (see Methods). Under these conditions, most islands exhibit straight edges, which indicates that they can only be of either  $zz$  or  $ac$  type. Topographic images with atomic resolution on both graphene and Ni are shown in Figure 2b,c. We observe that the TGIs have unreconstructed  $zz$  edges with no defects, in agreement with previous results.<sup>34,35</sup> The edge shown in Figure 2c runs perpendicular to the  $[1\bar{1}\bar{2}]$  direction, that is, parallel to a high symmetry  $[1\bar{1}0]$  direction of the Ni lattice. A honeycomb and an hexagonal lattice, representing the atomic positions of the graphene and surface Ni atoms, respectively, have been superposed on the image for illustrative purposes. Note that the STM image taken over the graphene-covered region

exhibits almost hexagonal contrast, despite the honeycomb atomic structure of graphene. This is a well-known electronic effect induced by the graphene–metal interaction, which breaks the symmetry between C atoms in on-top and hollow positions.<sup>46–48</sup> In particular, previous theoretical simulations concluded that, in the case of graphene on Ni(111), the bright spots in the STM images at zero or very small bias correspond to C atoms located in hollow positions,<sup>46,47</sup> as reproduced also by our calculations. Besides, all the images shown in this work have been acquired under well controlled tip conditions, which allows us to exclude tip-induced contrast effects. All this suggests that, away from local variations related, for example, to surface impurities, lattice imperfections, and the proximity of the edge, the spots with larger intensity in the STM images correlate with C atoms in hollow positions. In any case, the hexagonal units of the honeycomb lattice can be clearly identified and extrapolated to the Ni lattice, which let us draw two important conclusions: (i) that vertices of the honeycomb lattice at the graphene–Ni lateral boundary (red circles) correspond to hollow positions on the hexagonal lattice, and hence the edge is of  $zz_h$  type; (ii) the vertices representing the other sublattice (blue circles) are located on top of the Ni atoms, and hence, graphene has either top-fcc or top-hcp stacking with the substrate, in agreement with our initial hypothesis.

The great majority of the TGIs in our samples point in the same direction, as seen in Figure 2a. Because there is a one-to-one relationship between the edge type, stacking, and orientation of TGIs (Figure S2 of the Supporting Information), this implies that the TGIs have a preference for a unique edge type and stacking combination, which, according to our analysis, corresponds to  $zz_h$  and either top-fcc or top-hcp. Moreover, we find evidence that the edge type dominates the preference for the epitaxial stacking of the inner C atoms in the islands. The enlarged area of Figure 2a shows two TGIs pointing in opposite directions, meaning that they are rotated with respect to each other by 60°. This inverted orientation can only be explained by a change in the stacking or in the edge type (see Figure S2 of the Supporting Information). Note that all the TGIs pointing in the direction opposite to the predominant one (indicated by arrows in Figure 2a) have a small size, below 10 nm<sup>2</sup>. Since the effect of the edge type on the system's energy is higher for smaller islands, the most plausible scenario is that the TGIs with inverted orientation maintain the lowest energy edge configuration and change their stacking.

These experimental observations have been confirmed and complemented by DFT calculations. Figure 3 shows the model systems used in the simulations, namely TGIs with  $zz_t$  and  $zz_h$  edges and top-fcc or top-hcp stacking. The TGI and the top two Ni layers of a three layer Ni slab are fully relaxed, which leads to significant plastic deformation of the islands owing to edge-induced relaxations. These effects are expected to be significant in small size islands such as the one used here, where the size is imposed by computational limitations. However, results obtained on larger islands using a slab that contains only two metal planes confirm the edge energies obtained for the smaller TGIs (see Supporting Information). The relative energies of different edge types are calculated by subtracting the total energy of the TGIs shown in Figure 3 and dividing by the number of C atoms. This method neglects the plastic deformation of the islands, which would be difficult to disentangle by itself and that we estimate to have smaller

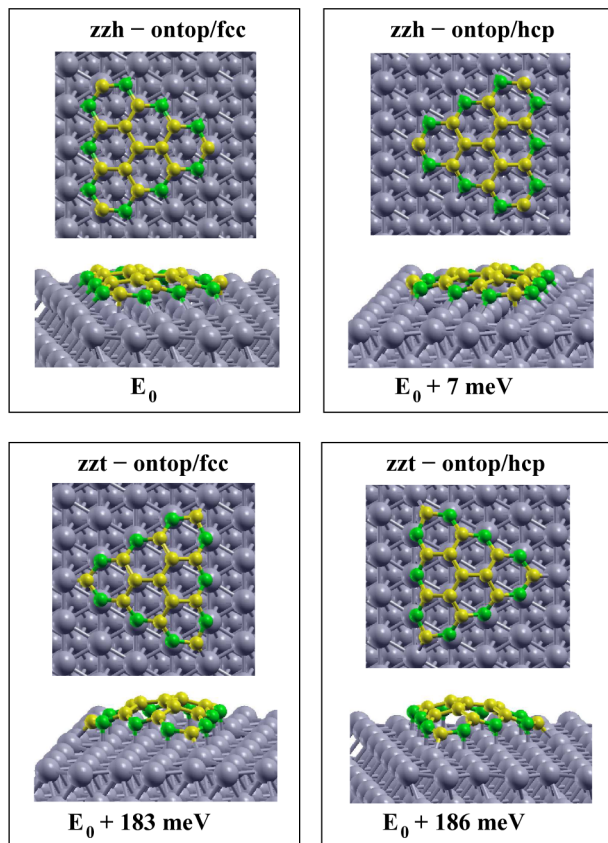


**Figure 3.** Relaxed model configurations of TGIs on Ni(111) calculated by DFT, together with the corresponding energies per C atom in meV. The latter are given with respect to  $E_0$ , the energy of the most stable TGI.

weight compared to edge effects. Our results indicate an energy difference of  $\sim 0.67$  eV between C-edge atoms in hollow and top positions. From this, we estimate an edge energy difference between  $zz_h$  and  $zz_t$  edges of  $\Delta E_{zz} \sim 0.27$  eV/ $\text{\AA}$  (see the Supporting Information for more details). This value might be overestimated because different edges induce different relaxations in the inner part of the islands. However, this effect should be mitigated for the calculations of larger islands reported in the Supporting Information. In the following, we use the average value of all these calculations to set the difference of the  $zz_h$  and  $zz_t$  edge energies, while our maximum and minimum values are used to associate an error bar with this result. According to this estimation  $\Delta E_{zz} = 0.22 \pm 0.05$  eV/ $\text{\AA}$ . Therefore, DFT predicts that the most stable TGIs have  $zz_h$

edges, in agreement with the experimental results. The preference for  $zz_h$  edges can be understood by considering the deformation of the  $sp^2$  hybridized orbitals of the edge C atoms as they bind to the surface Ni atoms. In the case of  $zz_h$  edges, only a small deformation is required to form a bond with a Ni atom, whereas for  $zz_t$  edges a larger deformation takes place, which also leads to the bent edge structure that can be observed in Figure 3.

With respect to the stacking with the substrate, the calculations predict a small energy gain for the top-fcc stacking with respect to the top-hcp, of the order of a few tens of meV per C atom, which is not very significant in the case of the small islands considered in this study. This result agrees with the calculations for extended graphene on Ni(111).<sup>43</sup> Moreover, it is consistent with the preferential orientation found for the TGIs. The small energy difference obtained for the two stacking configurations is reflected by the fact that islands with opposite orientation, although very rare, can still be observed when their size is small enough (Figure 2a).

Figure 4a shows that TGIs evolve into HGIs by annealing the Ni(111) surface up to 650 °C for 10 min. This seems to imply that the growth of the TGIs is kinetically limited, whereas the equilibrium shape of the graphene islands on Ni(111) is hexagonal, as confirmed by the results of our DFT simulations. This is similar to the homo- and heteroepitaxy of metals on (111) surfaces.<sup>49,50</sup> The triangular and hexagonal island shapes allow us to compare the structure and stability of different edge types. Contrary to TGIs, HGIs are constrained to exhibit  $zz_h$  and  $zz_t$  edges alternated along their perimeter. Because of the 60° angle between adjacent edges, the formation of ac edges can be excluded since these would be oriented at 30° with respect to the  $zz$  edges. As in the case of TGIs, HGIs have their edges aligned with the high symmetry directions of the substrate, and hence possess only  $zz$  edges. Since  $zz_h$  and  $zz_t$  edges alternate independently of the stacking (Figure 1), the edge energy contribution is equivalent for top-fcc and top-hcp stacking. The orientation of the islands does not change as they evolve from triangular to hexagonal by increasing the annealing temperature from 500 to 650 °C, which indicates that the preferential stacking for the HGIs and TGIs is the same, that is, top-fcc according to the DFT results. Figure 4b shows a detail of an HGI. Edges 1, 3, and 5 appear atomically straight and correspond to  $zz_h$  edges. Edges 2, 4, and 6, on the other hand, present a few structural imperfections and are shorter compared to the odd-numbered edges. These edges should be of the  $zz_t$  type according to the hard-sphere models presented in Figure 1. However, atomic resolution images of the HGI show that these edges undergo a reconstruction that has a periodicity of two benzene rings. This is clearly visible in Figure 4c, where an

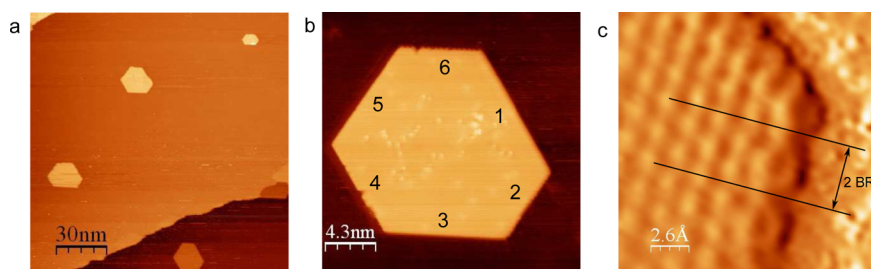


**Figure 4.** (a) Large area STM image of HGIs. Set point:  $I = 1.9$  nA,  $V_b = 2.1$  mV. (b) STM image of a single HGI. Set point:  $I = 9.6$  nA,  $V_b = 0.9$  mV. (c) Detail of a corner of the HGI shown in (b) with  $zz_h$  and  $zz_t$  (57) edges. The black lines in (c) illustrate the doubling of the periodicity observed in the reconstructed edge.

island corner is shown at the intersection of edges 1 and 2. We assign this reconstruction to a pentagon–heptagon  $zz(57)$  structure, which has a periodicity of two benzene rings and matches the observed atomic structure.

To confirm these results, we have performed extensive DFT calculations of graphene nanoribbons on Ni(111). Ribbons allow us to study two edge types simultaneously, as HGIs, but are computationally less demanding compared to hexagonal islands. In the following we only consider the  $zz(57)$  reconstruction, since the other known  $2 \times 2$  reconstruction of a  $zz$  edge, labeled as  $zz(ad)$  in ref 31, is energetically excluded by calculations shown in the Supporting Information. Figure 5

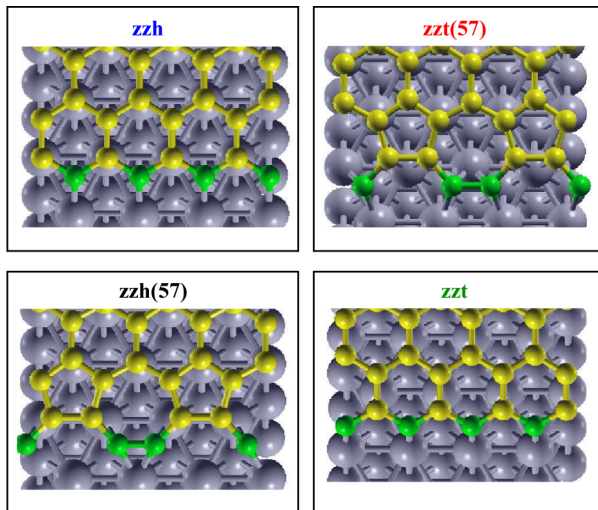


**Figure 5.** Relaxed edge structures calculated for graphene nanoribbons with a width of four benzene rings on Ni(111). For visualization purposes, the edge C atoms are represented in green.

presents the optimized structure of graphene nanoribbons with  $zz_h$ ,  $zz_h(57)$ ,  $zz_t$ , and  $zz_t(57)$  edges on Ni(111). For such structures, as described in detail in the Supporting Information, we obtain the following relationships between the energy of the four edge types:

$$\begin{aligned} E_{zzt(57)} &= E_{zzt} - 0.15 \text{ eV}/\text{\AA} \\ E_{zzh(57)} &= E_{zzh} + 0.16 \text{ eV}/\text{\AA} \\ E_{zzh(57)} + E_{zzt(57)} &= 1.07 \text{ eV}/\text{\AA} \end{aligned} \quad (1)$$

These numbers show that it is energetically favorable for  $zz_t$  edges to undergo the 57-reconstruction ( $E_{zzt(57)} < E_{zzt}$ ), whereas the opposite is true for  $zz_h$  edges ( $E_{zzh(57)} > E_{zzh}$ ), in agreement with the experimental observations.

From our calculations of the energetics of adsorbed nanoribbons it is only possible to obtain, once stacking is taken into account, three relations (eq 1) for four unknowns. Therefore, additional information is required to estimate the energy of the different edge types. Here we use our estimation of  $\Delta E_{zz}$  obtained from the calculations of the TGIs. In this way we obtain the edge energies represented in Figure 6a, where the edges with lowest energy are indeed the  $zz_h$  and  $zz_t(57)$  types.

The results of our calculations are in disagreement with recent theoretical studies of graphene nanoribbons on Ni(111),<sup>4,31</sup> in which the unreconstructed edge is predicted to be more stable than the reconstructed one. However, these studies do not consider the influence of stacking, which leads to

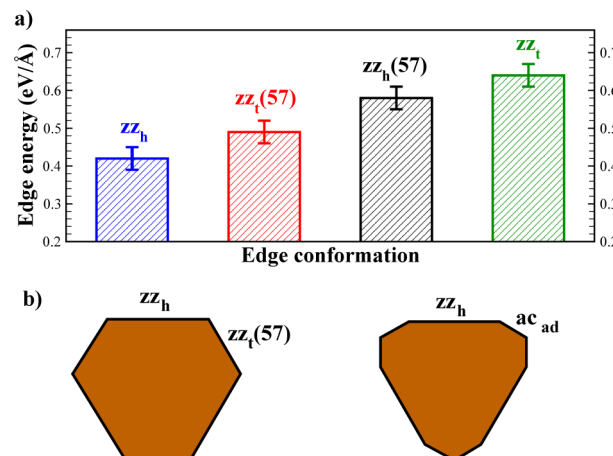


**Figure 6.** (a) Formation energies of graphene  $zz$  edges on Ni(111). (b) Equilibrium shape of graphene nanoislands on Ni(111) obtained by minimizing the edge energy. If edge reconstruction is allowed, the islands exhibit  $zz_h$  and reconstructed  $zz_t(57)$  edges, adopting a hexagon-like shape. If reconstruction is inhibited, the islands have a triangle-like shape and exhibit  $zz_h$  and reconstructed armchair edges.

the conclusion that the 57-reconstructed edges are always less stable than the unreconstructed ones. Besides, at least in one of these works,<sup>4</sup> the estimation of the edge formation energies is based on the assumption that the ribbons are perfectly symmetric, which is not true if epitaxial stacking is taken into account (see Figure S4 of the Supporting Information). However, it is interesting to note that the average value (over the two stacking configurations) of our edge energies is in good agreement with the values reported by Gao et al.<sup>31</sup> using plane-wave calculations and the same exchange-correlation functional that we use here (Perdew, Burke, and Ernzerhof functional,<sup>51</sup> see the Supporting Information). The agreement is particularly good for the unreconstructed zigzag edges, for which our average edge energy is  $0.53 \text{ eV}/\text{\AA}$ , exactly the value reported by Gao et al. for the zigzag edge energy (without resolving the stacking dependency). Our average value for the 57-reconstructed edge energies is  $\sim 0.54 \text{ eV}/\text{\AA}$ , which is somewhat lower than the  $0.60 \text{ eV}/\text{\AA}$  reported by Gao et al., but still in good correspondence.

With the edge energies in Figure 6a, following the classical Wulff construction, the equilibrium shape of graphene islands on Ni(111) turns out to be hexagonal, as shown in Figure 6b. The different length of the  $zz_h$  and  $zz_t(57)$  island edges observed in Figure 4b can also be accounted for by such a model and reflect the larger stability of  $zz_h$  edges as compared to  $zz_t(57)$  edges. On the other hand, if no reconstruction would occur for the  $zz_t$  edge, the islands would have an almost triangular shape, as shown in Figure 6b (the optimal shape calculated for triangular islands exhibits also portions of reconstructed armchair instead of  $zz_t$  edges, see the Supporting Information for more details).

These results outline a possible scenario to explain the evolution of TGIs into HGIs on Ni(111) when the annealing temperature is increased from  $\sim 500^\circ\text{C}$  to  $\sim 650^\circ\text{C}$ . According to our theoretical model, HGIs with alternate  $zz_h$  and  $zz_t(57)$  edges have lower energy compared to TGIs of equal size (we estimate HGIs of  $10 \text{ nm}^2$  to be  $\sim 3 \text{ eV}$  more stable than TGIs of the same size, see the Supporting Information). This suggests that an energy barrier must be overcome in order to achieve the equilibrium hexagonal shape. In view of our results, we can

speculate that this energy barrier is associated with the  $S7$ -reconstruction of the  $zz$  edges. Below a certain temperature the system does not have enough energy to overcome this barrier and, as a result, the  $zz_t$  edge does not reconstruct and the island grows into a triangle. On the contrary, as the temperature increases, the barrier can be easily surpassed and the  $zz_t$  edges efficiently reconstruct into  $zz_t(57)$ , giving rise to hexagonal nanoislands.

## CONCLUSIONS

In summary, we have shown that the structure and stability of the edges of graphene islands grown on Ni(111) are dominated by the stacking of the edge atoms relative to the substrate. Conversely, the edge type and energetics determine the island shape and, in TGIs smaller than  $10\text{ nm}^2$ , also the stacking relationship of the inner C atoms with the substrate. Atomically resolved STM images show that TGIs and HGIs exhibit only  $zz$ -like edges. As the epitaxial constraint imposed by the Ni substrate breaks the 6-fold symmetry of free-standing graphene, we distinguish between  $zz_h$  and  $zz_t$  edges, which differ in the position of the outermost C atoms relative to the substrate lattice. TGIs are bound uniquely by  $zz_h$  edges, whereas HGIs are bound by alternate  $zz_h$  and reconstructed  $zz_t(57)$  edges. Accordingly, DFT calculations show that the energy of the  $zz_h$  and  $zz_t(57)$  edges is about  $0.2\text{ eV}/\text{\AA}$  smaller relative to the unreconstructed  $zz_t$  edges, which are not stable on this surface. The edge energetics fully accounts for the shape of the HGIs observed experimentally and suggests that the temperature driven transition from TGIs to HGIs is an activated process related to the existence of an energy barrier for the  $S7$  pentagon-heptagon reconstruction. The stacking of the TGIs and HGIs is experimentally determined to be either top-fcc or top-hcp. All the TGIs and HGIs larger than a few  $\text{nm}^2$  adopt the same stacking, which, according to DFT, corresponds to the top-fcc configuration. The above considerations are important when a well-defined  $1 \times 1$  stacking leads to strongly orientation-dependent edge-stacking configuration, as is the case of Ni(111) or Co(0001).<sup>30</sup> This can apply in a different degree also to other close-packed metal surfaces. Likewise, the stability of  $zz$  edges and their tendency to reconstruct may play a role in determining the density and orientation of grain boundaries in extended graphene layers grown on metal substrates.

## ASSOCIATED CONTENT

### Supporting Information

The atomic structures and symmetry of different edge types, TGIs, and HGIs, as well as details of the DFT calculations. This material is available free of charge via the Internet at <http://pubs.acs.org>.

## AUTHOR INFORMATION

### Corresponding Authors

\*E-mail: wmbgalea@lg.ehu.es.

\*E-mail: marolle@gmail.com.

### Notes

The authors declare no competing financial interest.

## ACKNOWLEDGMENTS

We acknowledge support from the Basque Departamento de Educación, UPV/EHU (Grant No. IT-756-13), the Spanish Ministerio de Ciencia e Innovación (Grant Nos. MAT2013-

46593-C6-2-P and MAT2013-46593-C6-5-P, MAT2007-62732), the ETORTEK program funded by the Basque Departamento de Industria, the European Union FP7-ICT Integrated Project PAMS under Contract No. 610446, the European Research Council (StG 203239 NOMAD), and Agència de Gestió d'Ajuts Universitaris i de Recerca (2014 SGR 715).

## REFERENCES

- (1) Loginova, E.; Bartelt, N.; Feibelman, P.; McCarty, K. Factors Influencing Graphene Growth on Metal Surfaces. *New J. Phys.* **2009**, *11*, 063046.
- (2) Wofford, J. M.; Nie, S.; McCarty, K. F.; Bartelt, N. C.; Dubon, O. D. Graphene Islands on Cu Foils: The Interplay between Shape, Orientation, and Defects. *Nano Lett.* **2010**, *10*, 4890–4896.
- (3) Luo, Z.; Kim, S.; Kawamoto, N.; Rappe, A. M.; Johnson, A. T. C. Growth Mechanism of Hexagonal-Shape Graphene Flakes with Zigzag Edges. *ACS Nano* **2011**, *5*, 9154–9160.
- (4) Artyukhov, V. I.; Liu, Y.; Yakobson, B. I. Equilibrium at the Edge and Atomistic Mechanisms of Graphene Growth. *Proc. Natl. Acad. Sci. U.S.A.* **2012**, *109*, 15136–15140.
- (5) Ma, T.; Ren, W.; Zhang, X.; Liu, Z.; Gao, Y.; Yin, L.-C.; Ma, X.-L.; Ding, F.; Cheng, H.-M. Edge-Controlled Growth and Kinetics of Single-Crystal Graphene Domains by Chemical Vapor Deposition. *Proc. Natl. Acad. Sci. U.S.A.* **2013**, *110*, 20386–20391.
- (6) Nakada, K.; Fujita, M.; Dresselhaus, G.; Dresselhaus, M. S. Edge State in Graphene Ribbons: Nanometer Size Effect and Edge Shape Dependence. *Phys. Rev. B* **1996**, *54*, 17954–17961.
- (7) Brey, L.; Fertig, H. A. Edge States and the Quantized Hall Effect in Graphene. *Phys. Rev. B* **2006**, *73*, 195408–1–195408–5.
- (8) Barone, V.; Hod, O.; Scuseria, G. E. Electronic Structure and Stability of Semiconducting Graphene Nanoribbons. *Nano Lett.* **2006**, *6*, 2748–2754.
- (9) Ritter, K. A.; Lyding, J. W. The Influence of Edge Structure on the Electronic Properties of Graphene Quantum Dots and Nanoribbons. *Nat. Mater.* **2009**, *8*, 235–242.
- (10) Son, Y.-W.; Cohen, M. L.; Louie, S. G. Energy Gaps in Graphene Nanoribbons. *Phys. Rev. Lett.* **2006**, *97*, 216803–1–216803–4.
- (11) Han, M. Y.; Özilmez, B.; Zhang, Y.; Kim, P. Energy Band-Gap Engineering of Graphene Nanoribbons. *Phys. Rev. Lett.* **2007**, *98*, 206805–1–206805–4.
- (12) Fernández-Rossier, J.; Palacios, J. J. Magnetism in Graphene Nanoislands. *Phys. Rev. Lett.* **2007**, *99*, 177204–1–177204–4.
- (13) García-Lekue, A.; Balashov, T.; Olle, M.; Ceballos, G.; Arnau, A.; Gambardella, P.; Sanchez-Portal, D.; Mugarza, A. Spin-Dependent Electron Scattering at Graphene Edges on Ni(111). *Phys. Rev. Lett.* **2014**, *112*, 066802–1–066802–5.
- (14) Gan, Y.; Sun, L.; Banhart, F. One- and Two-Dimensional Diffusion of Metal Atoms in Graphene. *Small* **2008**, *4*, 587–591.
- (15) Cervantes-Sodi, F.; Csányi, G.; Piscanec, S.; Ferrari, A. C. Edge-Functionalized and Substitutionally Doped Graphene Nanoribbons: Electronic and Spin Properties. *Phys. Rev. B* **2008**, *77*, 165427–1–165427–13.
- (16) Wang, X.; Dai, H. Etching and Narrowing of Graphene from the Edges. *Nat. Chem.* **2010**, *2*, 661–665.
- (17) Gránas, E.; Knudsen, J.; Schröder, U. A.; Gerber, T.; Busse, C.; Arman, M. A.; Schulte, K.; Andersen, J. N.; Michely, T. Oxygen Intercalation under Graphene on Ir(111): Energetics, Kinetics, and the Role of Graphene Edges. *ACS Nano* **2012**, *6*, 9951–9963.
- (18) Novoselov, K. S.; Geim, A. K.; Morozov, S. V.; Jiang, D.; Zhang, Y.; I. V. Grigorieva, S. V. D.; Firsov, A. A. Electric Field Effect in Atomically Thin Carbon Films. *Science* **2004**, *306*, 666–669.
- (19) Datta, S. S.; Strachan, D. R.; Khamis, S. M.; Johnson, A. T. C. Crystallographic Etching of Few-Layer Graphene. *Nano Lett.* **2008**, *8*, 1912–1915.

- (20) Koskinen, P.; Malola, S.; Häkkinen, H. Self-Passivating Edge Reconstructions of Graphene. *Phys. Rev. Lett.* **2008**, *101*, 115502–1–115502–4.
- (21) Wassmann, T.; Seitsonen, A. P.; Saitta, A. M.; Lazzeri, M.; Mauri, F. Structure, Stability, Edge States, and Aromaticity of Graphene Ribbons. *Phys. Rev. Lett.* **2008**, *101*, 096402–1–096402–4.
- (22) Huang, B.; Liu, M.; Su, N.; Wu, J.; Duan, W.; Gu, B.-L.; Liu, F. Quantum Manifestations of Graphene Edge Stress and Edge Instability: A First-Principles Study. *Phys. Rev. Lett.* **2009**, *102*, 166404–1–166404–4.
- (23) Girit, C. O.; Meyer, J. C.; Erni, R.; Rossell, M. D.; Kisielowski, C.; Yang, L.; park, C. H.; Crommie, M. F.; Cohen, M. L.; Louie, S. G.; et al. Graphene at the Edge: Stability and Dynamics. *Science* **2009**, *323*, 1705–1708.
- (24) Koskinen, P.; Malola, S.; Häkkinen, H. Evidence for Graphene Edges Beyond Zigzag and Armchair. *Phys. Rev. B* **2009**, *80*, 073401–1–073401–3.
- (25) Rutter, G. M.; Guisinger, N. P.; Crain, J. N.; First, P. N.; Stroscio, J. A. Edge Structure of Epitaxial Graphene Islands. *Phys. Rev. B* **2010**, *81*, 245408–1–245408–4.
- (26) Chen, Y.-C.; de Oteyza, D. G.; Pedramrazi, Z.; Chen, C.; Fischer, F. R.; Crommie, M. F. Tuning the Band Gap of Graphene Nanoribbons Synthesized from Molecular Precursors. *ACS Nano* **2013**, *7*, 6123–6128.
- (27) Leicht, P.; Zielke, L.; Bouvron, S.; Moroni, R.; Voloshina, E.; Hammerschmidt, L.; Dedkov, Y. S.; Fonin, M. In Situ Fabrication Of Quasi-Free-Standing Epitaxial Graphene Nanoflakes On Gold. *ACS Nano* **2014**, *8*, 3735–3742.
- (28) Phark, S.-h.; Borme, J.; Vanegas, A. L.; Corbetta, M.; Sander, D.; Kirschner, J. Atomic Structure and Spectroscopy of Graphene Edges on Ir(111). *Phys. Rev. B* **2012**, *86*, 045442–1–045442–4.
- (29) Li, Y.; Subramanian, D.; Atodiresei, N.; Lazić, P.; Caciuc, V.; Pauly, C.; Georgi, A.; Busse, C.; Liebmann, M.; Blügel, S.; et al. Absence of Edge States in Covalently Bonded Zigzag Edges of Graphene on Ir(111). *Adv. Mater.* **2013**, *25*, 1967–1972.
- (30) Prezzi, D.; Eom, D.; Rim, K. T.; Zhou, H.; Xiao, S.; Nuckolls, C.; Heinz, T. F.; Flynn, G. W.; Hybertsen, M. S. Edge Structures for Nanoscale Graphene Islands on Co(0001) Surfaces. *ACS Nano* **2014**, *8*, 5765–5773.
- (31) Gao, J.; Zhao, J.; Ding, F. Transition Metal Surface Passivation Induced Graphene Edge Reconstruction. *J. Am. Chem. Soc.* **2012**, *134*, 6204–6209.
- (32) Tetlow, H.; de Boer, J. P.; Ford, I.; Vvedensky, D.; Coraux, J.; Kantorovich, L. Growth of Epitaxial Graphene: Theory and Experiment. *Phys. Rep.* **2014**, *542*, 195–295.
- (33) Merino, P.; Rodrigo, L.; Pinardi, A. L.; Méndez, J.; López, M. F.; Pou, P.; Pérez, R.; Martín Gago, J. A. Sublattice Localized Electronic States in Atomically Resolved Graphene-Pt(111) Edge-Boundaries. *ACS Nano* **2014**, *8*, 3590–3596.
- (34) Li, M.; Hannon, J. B.; Tromp, R. M.; Sun, J.; Li, J.; Shenoy, V. B.; Chason, E. Equilibrium Shape of Graphene Domains on Ni(111). *Phys. Rev. B* **2013**, *88*, 041402–1–041402–4.
- (35) Ollé, M.; Ceballos, G.; Serrate, D.; Gambardella, P. Yield and Shape Selection of Graphene Nanoislands Grown on Ni(111). *Nano Lett.* **2012**, *12*, 4431–4436.
- (36) Ibach, H.; Erley, W.; Wagner, H. The Preexponential Factor in Desorption - {CO} on Ni(111). *Surf. Sci.* **1980**, *92*, 29–42.
- (37) Christmann, K.; Behm, R. J.; Ertl, G.; Van Hove, M. A.; Weinberg, W. H. Chemisorption Geometry of Hydrogen on Ni(111): Order and Disorder. *J. Chem. Phys.* **1979**, *70*, 4168–4184.
- (38) Horcas, I.; Fernández, R.; Gómez-Rodríguez, J. M.; Colchero, J.; Gómez-Romero, J.; Baro, A. M. A Software for Scanning Probe Microscopy and a Tool for Nanotechnology. *Rev. Sci. Instrum.* **2007**, *78*, 013705–1–013705–8.
- (39) Soler, J. M.; Artacho, E.; Gale, J. D.; Garcia, A.; Junquera, J.; Ordejón, P.; Sanchez-Portal, D. The SIESTA Method for Ab Initio Order-N Materials Simulation. *J. Phys.: Condens. Matter* **2002**, *14*, 2745–2779.
- (40) Jacob, D.; Palacios, J. J. Critical Comparison of Electrode Models in Density Functional Theory Based Quantum Transport Calculations. *J. Chem. Phys.* **2011**, *134*, 044118–1–044118–16.
- (41) Gamo, Y.; Nagashima, A.; Wakabayashi, M.; Terai, M.; Oshima, C. Atomic Structure of Monolayer Graphite Formed on Ni(111). *Surf. Sci.* **1997**, *374*, 61–64.
- (42) Fuentes-Cabrera, M.; Baskes, M.; Melechko, A.; M, S. Bridge Structure for the Graphene/Ni(111) System: A First Principles Study. *Phys. Rev. B* **2008**, *77*, 035404–1–035404–10.
- (43) Lahiri, J.; Lin, Y.; Bozkurt, P.; Oleynik, I. I.; Batzill, M. An Extended Defect in Graphene as a Metallic Wire. *Nat. Nanotechnol.* **2010**, *5*, 326–329.
- (44) Zhao, W.; Kozlov, S. M.; Höfert, O.; Gotterbarm, K.; Lorenz, M.; Viñes, F.; Papp, C.; Görling, A.; Steinrück, H.-P. Graphene on Ni(111): Coexistence of Different Surface Structures. *J. Phys. Chem. Lett.* **2012**, *2*, 759–764.
- (45) Kozlov, S. M.; Viñes, F.; Görlan, A. Bonding Mechanisms of Graphene on Metal Surfaces. *J. Phys. Chem. C* **2012**, *116*, 7360–7366.
- (46) Bianchini, F.; Patera, L. L.; Peressi, M.; Africh, C.; Comelli, G. Atomic Scale Identification of Coexisting Graphene Structures on Ni(111). *J. Phys. Chem. Lett.* **2014**, *5*, 467–473.
- (47) Dzemiantsova, L. V.; Karolak, M.; Lofink, F.; Kubetzka, A.; Sachs, B.; von Bergmann, K.; Hankemeier, S.; Wehling, T. O.; Frömler, R.; Oepen, H. P.; et al. Multiscalar Magnetic Study of Ni(111) and Graphene on Ni(111). *Phys. Rev. B* **2011**, *84*, 205431–1–205431–10.
- (48) Varykhalov, A.; Marchenko, D.; Sánchez-Barriga, J.; Scholz, M. R.; Verberck, B.; Trauzettel, B.; Wehling, T. O.; Carbone, C.; Rader, O. Intact Dirac Cones at Broken Sublattice Symmetry: Photoemission Study of Graphene on Ni and Co. *Phys. Rev. X* **2012**, *2*, 041017–1–041017–10.
- (49) Michely, T.; Hohage, M.; Bott, M.; Comsa, G. Inversion of Growth Speed Anisotropy in Two Dimensions. *Phys. Rev. Lett.* **1993**, *70*, 3943–3946.
- (50) Kalff, M.; Comsa, G.; Michely, T. How Sensitive is Epitaxial Growth to Adsorbates? *Phys. Rev. Lett.* **1998**, *81*, 1255–1258.
- (51) Perdew, J. P.; Burke, K.; Ernzerhof, M. Generalized Gradient Approximation Made Simple. *Phys. Rev. Lett.* **1996**, *77*, 3865–3868.
- (52) Artyukhov, V. I.; Hao, Y.; Ruoff, R. S.; Yakobson, B. I. Breaking of Symmetry in Graphene. *Phys. Rev. Lett.* **2015**, <http://arxiv.org/abs/1405.5799>, (private communication).
- (53) Patera, L. L.; Bianchini, F.; Troiano, G.; Dri, C.; Cepek, C.; Peressi, M.; Africh, C.; Comelli, G. Temperature-Driven Changes of the Graphene Edge Structure on Ni(111): Substrate vs Hydrogen Passivation. *Nano Lett.* **2015**, *15*, 56–62.

## ■ NOTE ADDED IN PROOF

During the review process, we became aware of two related publications (refs 52 and 53). The computational work in ref 52, despite reporting slightly different results, confirms one of our main conclusions. Namely, the stacking of the edge atoms relative to the metal substrate plays a key role in the structure and stability of the graphene edge, and thus determines the shape of the graphene nanoislands. In ref 53, the periodicity doubling of the graphene edge was also experimentally observed, although it was attributed to hydrogen passivation in contrast to our present conclusions.